Geophysical Journal International

Geophys. J. Int. (2015) **200,** 1523–1537
GJI Seismology

doi: 10.1093/gji/ggu466

An effective method for small event detection: match and locate (M&L)

Miao Zhang[1] and Lianxing Wen[2,1]

[1]*Laboratory of Seismology and Physics of Earth's Interior; School of Earth and Space Sciences, University of Science and Technology of China, Hefei, Anhui* 230026*, P.R. China. E-mail: zhmiao@mail.ustc.edu.cn*
[2]*Department of Geosciences, State University of New York at Stony Brook, Stony Brook, NY* 11794*, USA*

Accepted 2014 December 2. Received 2014 October 11; in original form 2014 June 19

SUMMARY

Detection of low magnitude event is critical and challenging in seismology. We develop a new method, named the match and locate (M&L) method, for small event detection. The M&L method employs some template events and detects small events through stacking cross-correlograms between waveforms of the template events and potential small event signals in the continuous waveforms over multiple stations and components, but the stacking is performed after making relative traveltime corrections based on the relative locations of the template event and potential small event scanning through a 3-D region around the template. Compared to the current methods of small event detection, the M&L method places event detection to a lower magnitude level and extends the capability of detecting small events that have large distance separations from the template. The method has little dependence on the accuracy of the velocity models used, and, at the same time, provides high-precision location information of the detected small-magnitude events. We demonstrate the effectiveness of the M&L method and its advantage over the matched filter method using examples of scaled-down earthquakes occurring in the Japan Island and foreshock detection before the 2011 M_w 9.0 Tohoku earthquake. In the foreshock detection, the M&L method detects four times more events (1427) than the templates and 9 per cent (134) more than the matched filter under the same detection threshold. Up to 41 per cent (580) of the detected events are not located at the template locations with the largest separation of 9.4 km. Based on the identified foreshocks, we observe five sequences of foreshock migration along the trench-parallel direction toward the epicentre of the M_w 9.0 main shock.

Key words: Time-series analysis; Earthquake source observations; Seismic monitoring and test-ban treaty verification; Wave propagation.

1 INTRODUCTION

Detection of low magnitude events is important in many aspects of seismological studies, such as the determination of high-precision fault plane seismicity (Mori & Hartzell 1990; Dreger & Kaverina 2000; Kuge 2003; Kao & Shan 2007; Yang *et al.* 2009), foreshock activities preceding large earthquakes (Kato *et al.* 2012; Brodsky & Lay 2014), earthquake triggering (Hill *et al.* 1993; Kilb *et al.* 2000; Gomberg *et al.* 2001; Peng *et al.* 2010; Meng *et al.* 2013; Meng & Peng 2014), low-frequency earthquake detection within tremor (Shelly *et al.* 2006, 2007; Shelly 2010), monitoring micro-earthquakes induced by hydraulic fracturing (House 1987; Rutledge & Phillips 2003; Eisner *et al.* 2008; Anikiev *et al.* 2014), detecting low-yield nuclear tests (Shearer & Astiz 1997; Richards & kim 1997; Waldhauser *et al.* 2004; Wen & Long 2010; Zhang & Wen 2013), and locating trapped miners after a mine collapse (Cao *et al.* 2008; Hanafy *et al.* 2009), etc. Traditional methods of event identification, which rely on phase identification, are usually hindered by low signal-to-noise ratio (SNR) in small event recordings.

Two categories of the methods are most notable for small event detections: the source-scanning algorithm (SSA) and the matched filter technique. The SSAs identify events based on the stacked energy over some signal characteristics of a potential phase (e.g. the absolute amplitude, energy envelope or the short time average to long time average ratio (STA/LTA) of seismic waveforms, etc.) through a range of trial source location and origin time (e.g. Kao & Shan 2004, 2007; Gharti *et al.* 2010; Liao *et al.* 2012; Drew *et al.* 2013; Grigoli *et al.* 2013a,b; Langet *et al.* 2014). The matched filter technique employs some template events and detects small events through stacking cross-correlograms between waveforms of the template events and potential small event signals in the continuous waveforms over multiple stations and components

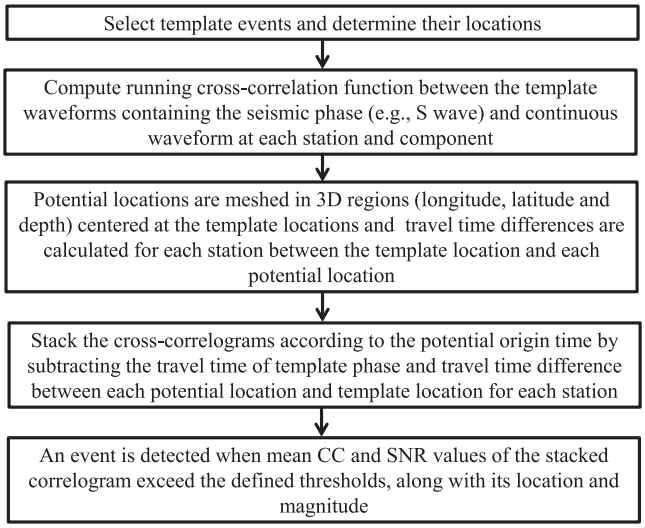

Figure 1. Flow diagram of the M&L method.

(Gibbons & Ringdal 2006; Gibbons *et al.* 2007; Shelly *et al.* 2007; Peng & Zhao 2009). The method takes advantage of the capability of cross-correlation technique to detect weak signal with similar waveform and is effective in detecting a similar signal in low SNR. It has been extensively applied in detecting low-frequency earthquakes within tremor (e.g. Shelly *et al.* 2007), aftershocks (e.g. Peng & Zhao 2009) and microseismic events induced by hydraulic fracturing (e.g. Eisner *et al.* 2008). However, these two categories of the methods still suffer some shortcomings. The SSA method may fail when the seismic signals are buried in the noise or mixed with other signals, limiting its detectable magnitude of small events. Besides, the traveltime correction of the trial source location significantly depends on the accuracy of the velocity model used. On the other hand, the matched filter method would require that the small events are colocated with one of the template events.

In this paper, we develop a new method, named match and locate (M&L), for small event detection. The method adopts similar concepts of waveform correlation detection in the matched filter method, but takes account of possible location difference of small events from the template. The M&L method makes the event detection more effective and high-precision event location information available at the same time. We introduce the method procedure and detection criteria in Section 2, illustrate its effectiveness, advantage over the matched filter technique and the location resolution of the detected events using the signals of two known earthquakes occurring in the Japan Island and the recorded background noise in Section 3, apply the method to detect the foreshocks before the 2011 M_w 9.0 Tohoku earthquake and compare our result with the matched filter in Section 4, and discuss the differences between different methods in Section 5.

2 M&L METHOD

2.1 Method procedure

Similar to the matched filter, the M&L method employs some template events and detects small events through stacking cross-correlograms between waveforms of the template events and potential small event signals in the continuous waveforms over multiple stations and components, but the stacking is performed after making relative traveltime corrections based on the relative locations of the template event and potential small event scanning through a 3-D region around the template. The procedure of the M&L method is illustrated schematically in Fig. 1. First, we select the template events and determine their locations (often from a catalogue). The template seismogram segments including the seismic phase with the strongest amplitude (usually the *S* wave in local and regional scales) are applied running cross-correlation with the continuous data stream at each station and data component. Potential locations are meshed in a 3-D region (longitude, latitude and depth) centred at the template locations. For each potential origin time and location of small event, we first align the cross-correlograms according to the traveltime of the reference phase and the traveltime difference predicted based on the relative location between the template and the potential location of small event, and then stack them for all stations and components. We compute the mean correlation coefficient (CC) value and SNR of the stacked cross-correlograms. When the mean CC and SNR values exceed the defined thresholds, we regard as a positive detection of a small event and the location with the maximum mean CC value is regarded as the location of the small event. Once an event is detected, its magnitude is computed based on the median value of the peak amplitude ratio between the detected event and the template event among all channels (Peng & Zhao 2009; Meng *et al.* 2013).

The traveltime difference Δt due to the location difference between the template and potential small event is calculated as follows (Wen 2006; Wen & Long 2010; Zhang & Wen 2013):

$$\Delta t(k, p) = \mathrm{d}D_k \frac{\mathrm{d}t}{\mathrm{d}D}(k, p, D, h) + \mathrm{d}h \frac{\mathrm{d}t}{\mathrm{d}h}(k, p, D, h), \quad (1)$$

$\mathrm{d}D_k$ is the difference in epicentral distance at station k due to the relative difference between the template and potential small event, $\mathrm{d}h$ relative depth change between the two events, and $\frac{\mathrm{d}t}{\mathrm{d}D}(k, p, D, h)$, $\frac{\mathrm{d}t}{\mathrm{d}h}(k, p, D, h)$ the derivatives of traveltime of the seismic phase p with respect to template epicentral distance D (horizontal slowness) and template depth h (vertical slowness), respectively. $\frac{\mathrm{d}t}{\mathrm{d}D}(k, p, D, h)$ and $\frac{\mathrm{d}t}{\mathrm{d}h}(k, p, D, h)$ can be calculated for each station and its associated seismic phase, using a 1-D reference earth's model. The calculation of traveltime difference $\Delta t(k, p)$ depends only slightly on the reference model, making our detection programs little affected by the reference model used.

Table 1. Earthquake parameters.

	Origin time (JST)	Latitude	Longitude	Depth	M
Template event[a]	2012/12/17 11:32:25.950	37.7578°N	139.9792°E	8.20 km	3.20
Slave event 1[a]	2012/07/17 11:40:28.390	37.7665°N	139.9807°E	8.42 km	3.20
Detected event 1[b]	2012/07/17 11:40:28.335	37.7672°N	139.9787°E	8.47 km	3.15
Slave event 2[a]	2012/02/20 21:21:15:000	37.8008°N	140.0245°E	8.47 km	3.20
Detected event 2[b]	2012/02/20 21:21:14.867	37.7991°N	140.0224°E	9.71 km	3.20

[a]Japan Meteorological Agency (JMA).
[b]M&L method.

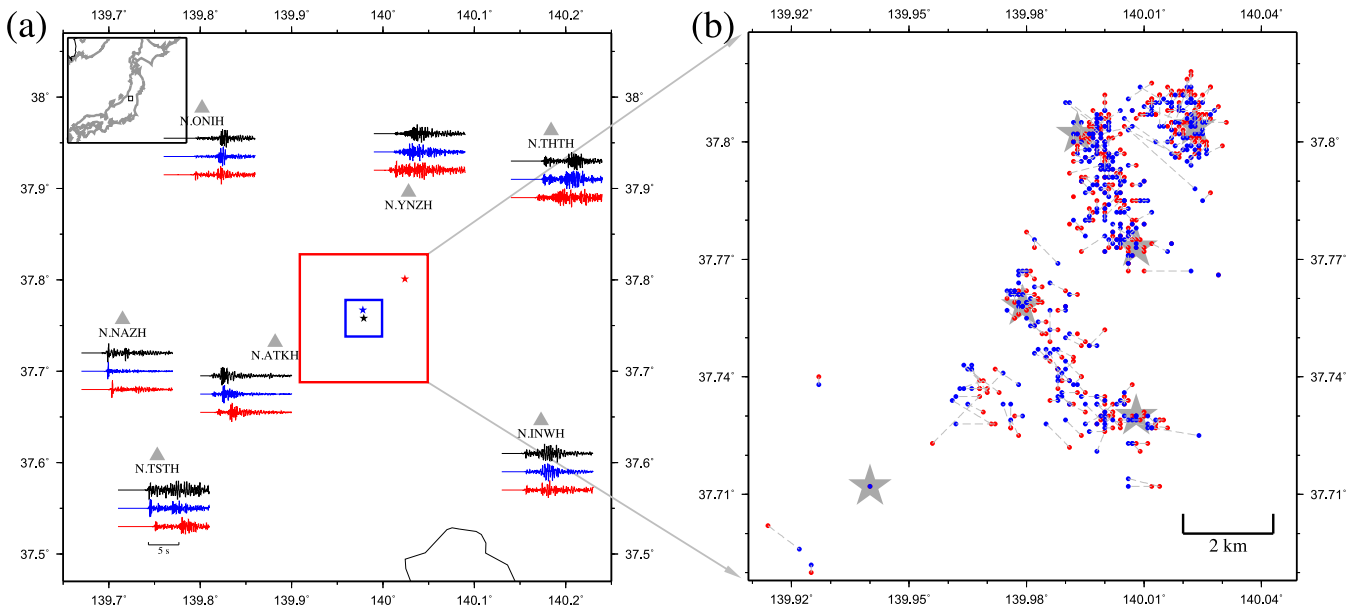

Figure 2. (a) Map showing stations (grey triangles), template earthquake (black star), slave earthquake 1 (blue star) and slave earthquake 2 (red star) shown in Table 1. The searched area is 0.04° × 0.04° in latitude and longitude and 2 km in depth (blue rectangle) for slave earthquake 1, and 0.14° × 0.14° and 4 km in depth (red rectangle) for slave earthquake 2, centred at the template earthquake location. The vertical component seismograms of the template event (black traces), slave event 1 (blue traces) and slave event 2 (red traces) are plotted close to the station symbols and names. Inset: the regional map of Japan, with the black rectangle indicating the study region. (b) M&L detected events (blue stars) and the JMA catalogue (red stars), with their correspondence linked by dashed grey lines, for a group of 360 earthquakes occurring within the red square area in Fig. 2(a). Six template events are marked by grey stars.

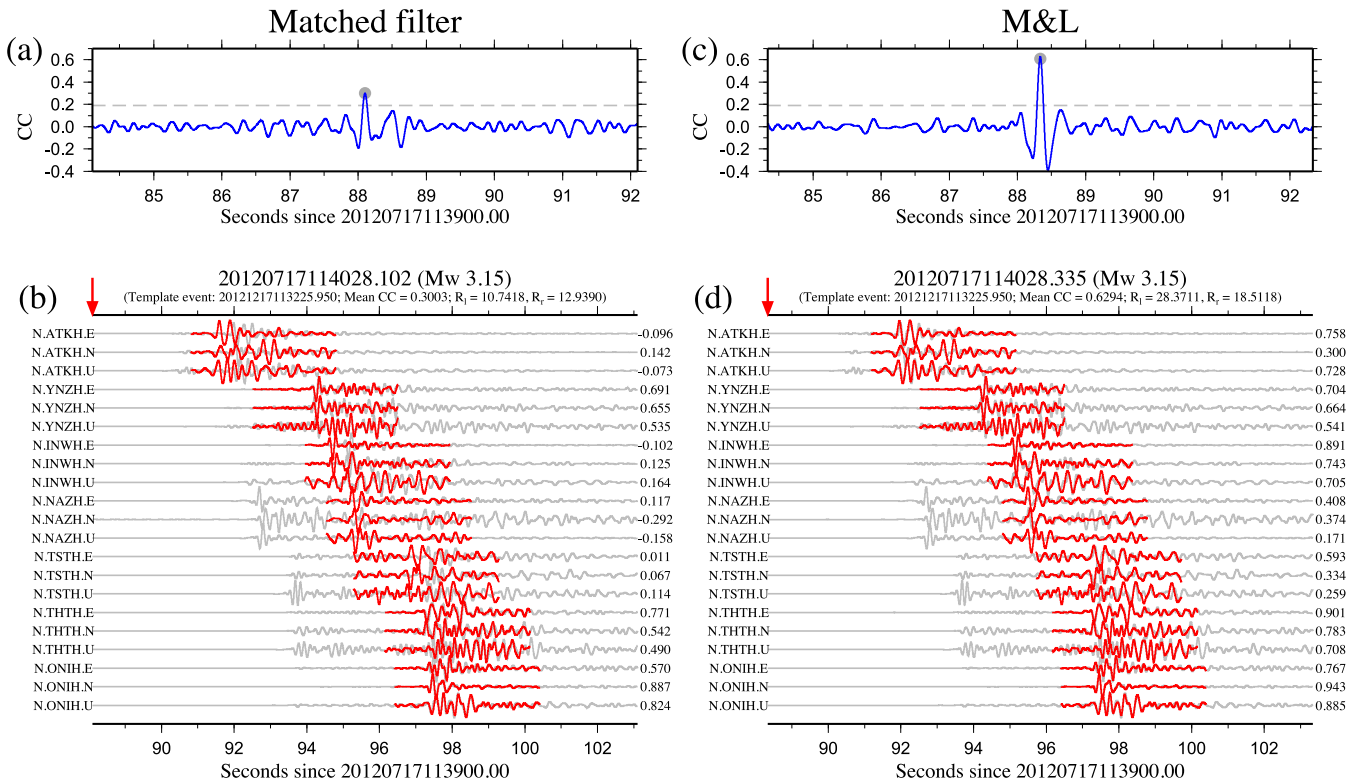

Figure 3. (a, c) Stacked cross-correlograms and (b, d) comparison of the template seismograms (red traces) with portions of the signals detected for slave earthquake 1 (Table 1) in the continuous waveforms (grey traces), between the matched filter (a, b) and the M&L method (c, d). Grey points in (a, c) and red arrows in (b, d) mark the determined origin time of the detected earthquake. The grey dashed lines in (a, c) indicate the mean CC threshold (0.19) of detection. Channel name and CC value are labelled on the left- and right-hand sides of each trace, respectively. The estimated magnitude, mean CC value and SNRs of the left (R_l) and right (R_r) portions of the correlograms are marked under the subtitles.

2.2 Detection criteria

As we mention above, the detection criteria include the mean CC value and SNR of the stacked cross-correlograms. We explain the reasoning of these criteria below, based on the approximate representation of cross-correlograms of two close events.

An observed seismogram $O(t)$ can be described as the convolution of these terms (Helmberger 1983):

$$O(\vec{r}, t) = I(t) * A(\vec{r}, t) * G(\vec{r}, t) * M(\phi_s, \delta, \lambda, i_\xi, \phi, t), \quad (2)$$

where $\vec{r}$ is the distance vector from source to station, $I(t)$ the seismic instrument response, $A(\vec{r}, t)$ the attenuation factor, $G(\vec{r}, t)$ the Green's function and $M(\phi_s, \delta, \lambda, i_\xi, \phi, t)$ the source term, which depends on strike ϕ_s, dip δ, rake λ, take-off angle i_ξ and azimuth ϕ.

For a point source, $M(\phi_s, \delta, \lambda, i_\xi, \phi, t)$ can be expressed by the product of a radiation pattern term F and the source time function $S(t)$, that is

$$M(\phi_s, \delta, \lambda, i_\xi, \phi, t) = F(\phi_s, \delta, \lambda, i_\xi, \phi)S(t). \quad (3)$$

The normalized cross-correlation of seismograms of two close events $[O_1(t), O_2(t)]$ is expressed by

$$NCC(t) = \frac{\int_{-T}^{T} O_1(\vec{r_1}, \tau)O_2(\vec{r_2}, t+\tau)\mathrm{d}\tau}{\sqrt{\int_{-T}^{T} O_1(\vec{r_1}, \tau)O_1(\vec{r_1}, t+\tau)\mathrm{d}\tau}\sqrt{\int_{-T}^{T} O_2(\vec{r_2}, \tau)O_2(\vec{r_2}, t+\tau)\,\mathrm{d}\tau}}, \quad (4)$$

where T corresponds to the length of time window of the reference phase.

The instrument response $I(t)$ is cancelled out in one common station. When two events occur in a close proximity (i.e. $\vec{r_1} \to \vec{r_2}$), the attenuation term $A(\vec{r}, t)$ and the Green's function $G(\vec{r}, t)$ also will be cancelled out because of the common propagation path. The CC value is determined by the normalized cross-correlation at the

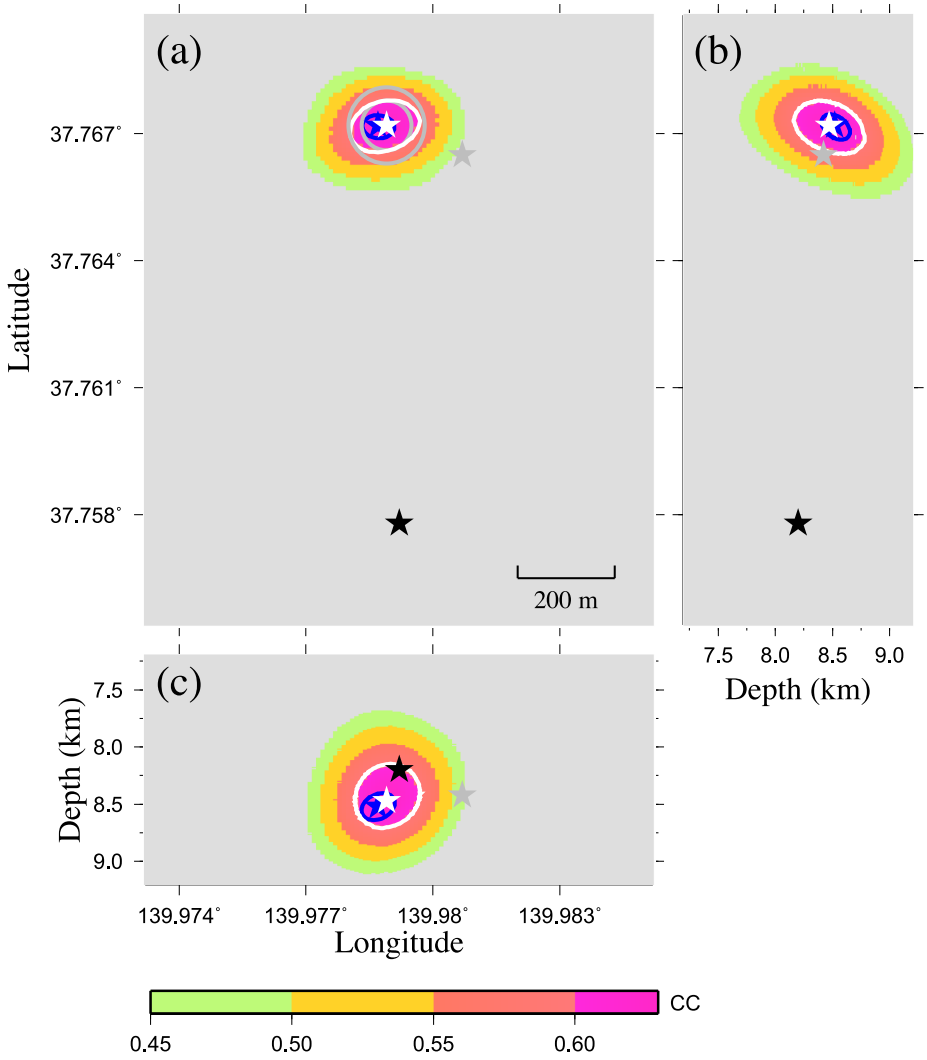

Figure 4. Mean CC value of the stacked correlogram as a function of assumed location of slave earthquake 1 (only the regions with CC > 0.45 are plotted) in three plane views: (a) longitude–latitude plane, (b) latitude–depth plane and (c) longitude–depth plane, along with the template location (black stars), M&L determined location (with the maximal CC value, white stars), the reference location (blue stars; determined using phase traveltime difference between the events by Wen (2006) method) and the JMA catalogue location (grey stars) of the slave event, the 95 per cent confidence ellipse of the reference location based on the chi-square distribution (blue ellipses, Fig. S1), and the confidence level of slave earthquake 1 location within 94.5 per cent of the maximal mean CC (white ellipses).

zero time lag point t_0 and is therefore:

$$NCC(t_0) \approx \frac{F_1 F_2 \int_{-T}^{T} S_1(\tau) S_2(t_0+\tau)\mathrm{d}\tau}{|F_1 F_2| \sqrt{\int_{-T}^{T} S_1(\tau) S_1(t_0+\tau)\mathrm{d}\tau} \sqrt{\int_{-T}^{T} S_2(\tau) S_2(t_0+\tau)\mathrm{d}\tau}}. \tag{5}$$

From eq. (5), we show that, when two events occur in a close proximity, only the difference in source time functions and the polarity difference in source radiation patterns would affect the CC value in one station. When two events possess same source time functions and same radiation patterns, CC value is 1. However, when source time functions of the two events differ, CC values will be less than one (even in the absence of noise and when two events possess same focal mechanisms).

As discussed above, we may miss detection of some events with different source time functions from the template event, if the detection criterion is only based on the mean CC values. Lowering the CC threshold may make those missing events detectable, however it would also increase the chance of false detection. The cross-correlograms between events with different source time functions have relatively low CC values, but with relatively high SNRs. We thus combine the SNRs in event detection, special for the cases of small mean CC values.

At any given time t, the SNR of the stacked correlogram is evaluated by the ratios of the CC value at the time to the average background CC values in time windows in the left and right vicinities of t. Similar to Gibbons & Ringdal (2006), we define them as left (R_l) and right (R_r) SNRs, and more specifically:

$$\begin{aligned} R_l(t) &= \frac{C(t)}{\overline{C_l(t)}}, \quad \overline{C_l(t)} = \frac{\sum_{t' \in I_l} |C(t')|}{\sum_{t' \in I_l} 1} \\ R_r(t) &= \frac{C(t)}{\overline{C_r(t)}}, \quad \overline{C_r(t)} = \frac{\sum_{t' \in I_r} |C(t')|}{\sum_{t' \in I_r} 1} \end{aligned} \tag{6}$$

the left and right time intervals I_l and I_r are specified as:

$$I_l = [t-b, t-a], \; I_r = [t+a, t+b], \text{ with } 0 < a < b, \tag{7}$$

where $C(t)$ is the stacked cross-correlation function, the values for a and b are the starting and ending times (from the maximum mean CC value) of the time windows used to define SNRs and

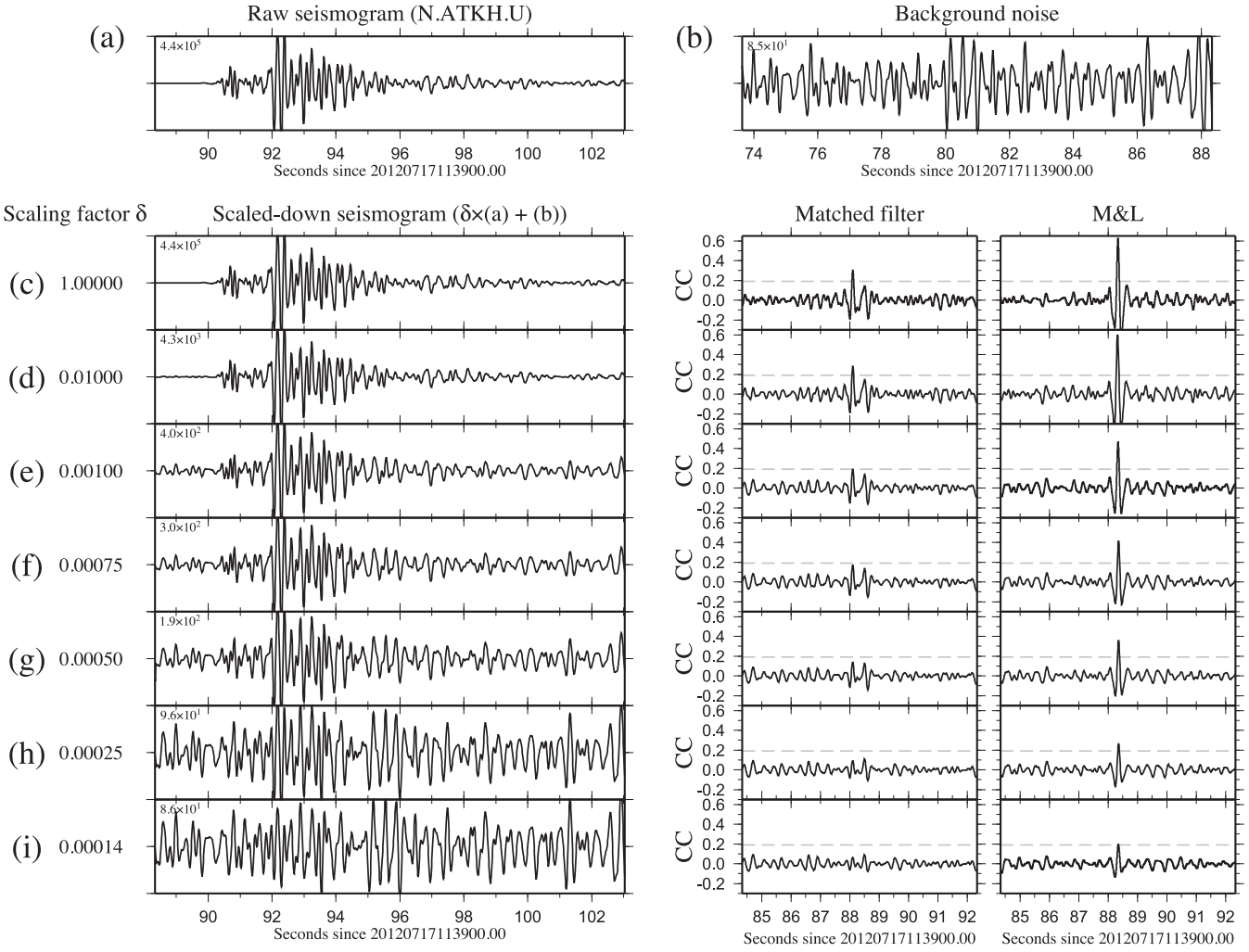

Figure 5. (a) An example vertical component of seismogram of an event recorded at station N.ATKH, (b) background noise taken before the arrival of seismic signals in the same channel, left-hand panels of (c)–(i): seismograms obtained by multiplying the signal seismogram in (a) by a scaling factor δ (values are labelled at the left of the corresponding seismograms) and superimposing the background noise in (b), and right-hand panels of (c)–(i): corresponding stacked cross-correlograms for the matched filter and the M&L methods between the template seismograms and scaled-down signals with noise in the left-hand panels of (c)–(i). Maximum amplitudes of seismograms are marked in top-left of each panel in (c)–(i). The mean CC threshold (0.19) is marked with the grey dashed lines in the right-hand panels of (c)–(i).

are determined empirically. The value of a is chosen according to the width of the 'side-lobes', which is caused by the correlation of finite-frequency signals. The value of b should be large enough to provide a sufficiently long time window $|b - a|$ to measure the relatively stable background CCs in the left and right vicinities of the maximum value (Gibbons & Ringdal 2006). Certainly, the frequency range would affect the selection of these two parameters. Typical values of the constants a and b are 1.0 and 3.0 s used in this paper.

The criteria of event detection are based on the mean CC values and SNRs of the stacked correlogram. Once the mean CC and SNRs (R_l and R_r) exceed the defined mean CC and SNR (R_l^0 and R_r^0) thresholds, one event is detected. The SNR threshold depends on mean CC, average background CC and a coefficient α that is a function of mean CC. Specifically, the left and right SNRs thresholds are defined by

$$R_l^0(t) = \alpha_l \frac{C(t)}{\overline{C_l^0}}, \quad R_r^0(t) = \alpha_r \frac{C(t)}{\overline{C_r^0}}, \tag{8}$$

where $\overline{C_l^0}$ and $\overline{C_r^0}$ are the left and right average background CCs, which are estimated from the left and right average background CCs of all template self-detections. To detect as many events and reduce the chance of false detection (special for the cases of small mean CC values), the detection criteria are set as follows: (1) when mean CC value is large (in the present data application, larger than nine times of the background mean CC value), only the mean CC threshold is applied and (2) when mean CC value is small (in the present data application, smaller than nine times but larger than seven times of the background mean CC value), both the mean CC and SNR thresholds are used. When applying the SNR threshold, the left and right SNR coefficients α_l and α_r are also selected to be a function of mean CC value (i.e. the smaller mean CC, the larger α_l and α_r values). An example of the choosing of these parameters is given in Section 4.

Like the matched filter method, there is some trade-off between increasing the number of detections (by lowing the detection threshold) and increasing the likelihood of some false detections in the M&L detection. In other words, with a lower mean CC threshold, the number of the detected events would increase, but so would the likelihood of some false detections. Introducing an additional SNR threshold in the case of small mean CC values alleviates this problem and allows the capture of desired detections from nearby events with different source–time functions. In addition, to avoid multiple counts, only the one with the highest mean CC value is kept in a certain time window (e.g. 6 s used in this paper).

3 ROBUSTNESS TEST OF THE M&L METHOD AND ITS COMPARISON WITH THE MATCHED FILTER METHOD

3.1 Effectiveness of the M&L method

We illustrate the effectiveness of the M&L method and its comparison with the matched filter method using the observed waveforms of three earthquakes (20121217, 20120717 and 20120220) occurring in the Japan Island (Table 1) as well as the recorded background noise. We use event 20121217 as the template event and events 20120717, 20120220 as slave events 1 and 2 (i.e. events to be detected; Table 1). Based on the Japan Meteorological Agency (JMA) catalogue, slave events 1 and 2 are 1.0 and 6.2 km away from the template event, respectively (Fig. 2). The observed waveforms in the seven nearest three-component Hi-net stations (21 channels) are used (Fig. 2). Seismic data are band-pass filtered from 2 to 8 Hz. The searched area for the potential slave event location is 0.04° in latitude and 0.04° in longitude with a searching interval of 0.0001°, and 2 km in depth with a searching interval of 0.01 km, centred at the template location. Waveforms of Sg wave are used and Sg phase is adopted in the relocation procedure based on the 1-D JMA2001 velocity model (Ueno *et al.* 2002). A 4-s time window (1 s before and 3 s after the predicted Sg wave arrival) is used as the template waveform window.

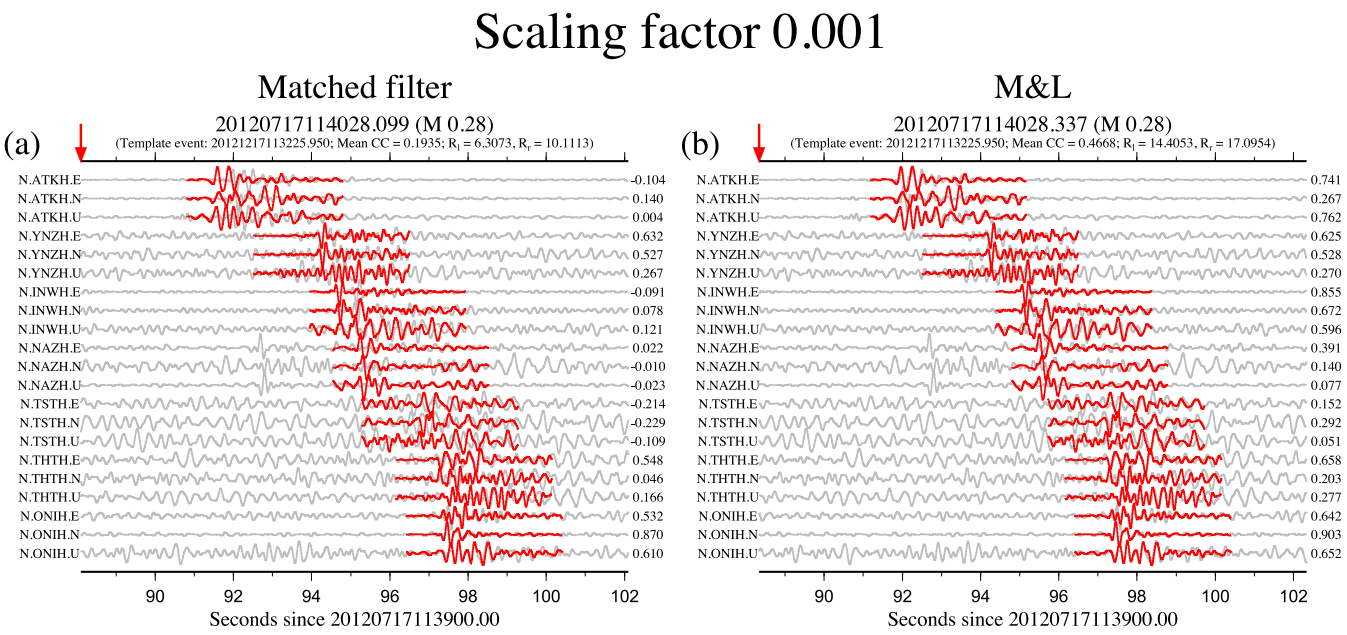

Figure 6. Comparisons of template seismograms (red traces) with portion of the seismic signal detected in the continuous waveform data (grey traces) between the matched filter (left-hand panel) and M&L (right-hand panel) for the case of a scaling factor of 0.001 in Fig. 5(e). The determined origin time, mean CC, and SNRs are marked under the corresponding titles, and the origin time is labelled by red arrows.

With an empirical mean CC threshold of 0.19, both M&L and matched filter detect slave event 1 (Fig. 3). The M&L method places slave event 1 at (37.7672°N, 139.9787°E) with a depth of 8.47 km and a magnitude of 3.15, close to the event parameters provided by JMA (Table 1). The matched filter detects the event with a smaller stacked mean CC value of 0.3003 (*cf.* 0.6294 by the M&L method) and smaller SNRs (Fig. 3). The stacked cross-correlogram in the M&L method also exhibits a more impulsive shape, indicating that energy is more coherent in time in the individual stacked correlogram. The maximum mean CC value in the M&L detection is well localized in a small region in the mean CC distribution over all potential locations (Fig. 4), indicating reliable detection and high resolution relocation of the slave event.

We scale-down the signals (multiplying the signals by a scaling factor) and superimpose them with the background noise, to simulate the cases of low-magnitude earthquake detection. 15 s of seismic noise before event origin time is superimposed on the scaled-down signal seismograms (Fig. 5). With an empirical threshold mean CC of 0.19, the matched filter no longer detects the slave event when the scaling factor is smaller than 0.001 (Figs 5e and 6), which corresponds to an event of 0.2 in magnitude. With the same detection threshold, the M&L method is able to detect the event up to a scaling factor of 0.00014, corresponding to an event of –0.65 in magnitude (Figs 5i and 7). In the M&L detection limit, the signals are buried in the background noise and no longer identifiable by eye (Figs 5i and 7).

As we show above, both the matched filter and the M&L method are able to detect the events that are in close proximity of the template (e.g. <2 km), although with different detection limits of event magnitude. However, when the separation of slave event location from the template events is larger (e.g. >4 km), the matched filter method would no longer work. This is illustrated in the example of slave event 2 (Fig. 8). Because of the large separation between the template and the slave event, the cross-correlograms of different stations are not aligned coherently in time and stacking would no longer enhance the signal-to-noise ratio of the correlograms, leading to the failure in the matched filter detection. However, it can be robustly detected by the M&L method (Fig. 8), as the optimal search for potential location of the slave event in the M&L method

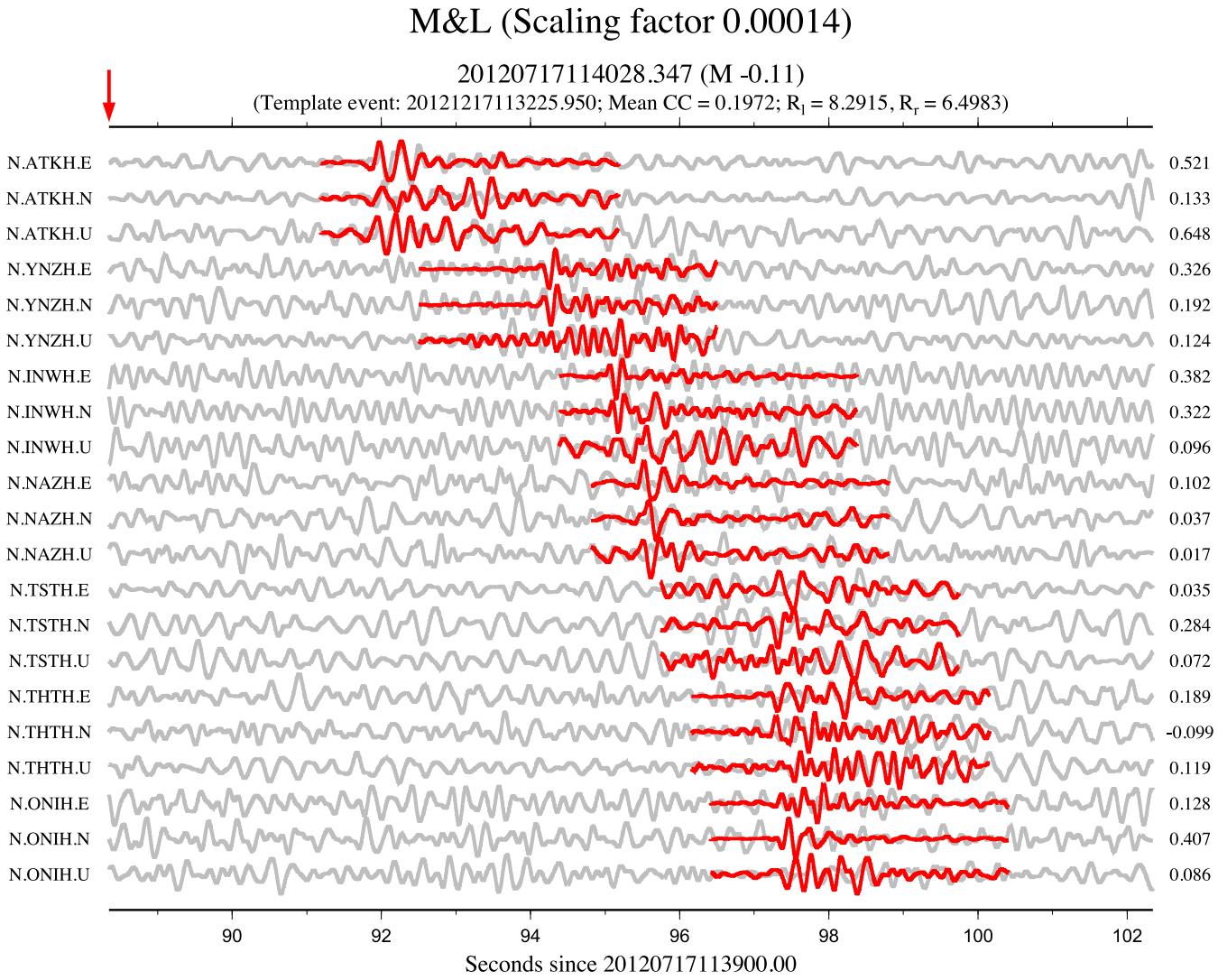

Figure 7. Comparisons of template seismograms (red traces) with portion of the seismic signal detected in the continuous waveform data (grey traces) in M&L for the case of a scaling factor of 0.00014 in Fig. 5(i). The determined origin time, mean CC, and SNRs are marked under the corresponding titles, and the origin time is labelled by red arrow.

makes effective traveltime corrections so that the correlograms are stacked coherently in time.

We further check the robustness of the M&L method using a catalogue of events that are clearly identified. We apply the M&L method to detect a group of 360 earthquakes in JMA catalogue. These earthquakes have a magnitude larger than 2.0 and occurred within a 0.14° × 0.14° area in the Japan Island in 2012 (red square in Fig. 2a). Six templates are chosen based on their spatial distribution. The M&L method recovers 348 of the 360 earthquakes (Fig. 2b). 12 events escape the detection, because they occurred within a 6 s interval with other events and are not regarded as independent events (e.g. 20120902024803 and 20120902024804). The determined magnitudes are also very close to, but systematically 4 per cent lower than, the JMA catalogue. The difference may be caused by the frequency difference used in the magnitude determination between the two methods. The detection is so robust that even if we scale down the signals of these 348 earthquakes to the level of background noise, which corresponds to a magnitude of –0.28 in average, 97 per cent of the earthquakes are still in the detection.

3.2 Location resolution of the M&L detection

Direct estimate of location uncertainty for each individual M&L detection becomes impossible, as signals of many detected events are weak and some are even buried in the background noise. The

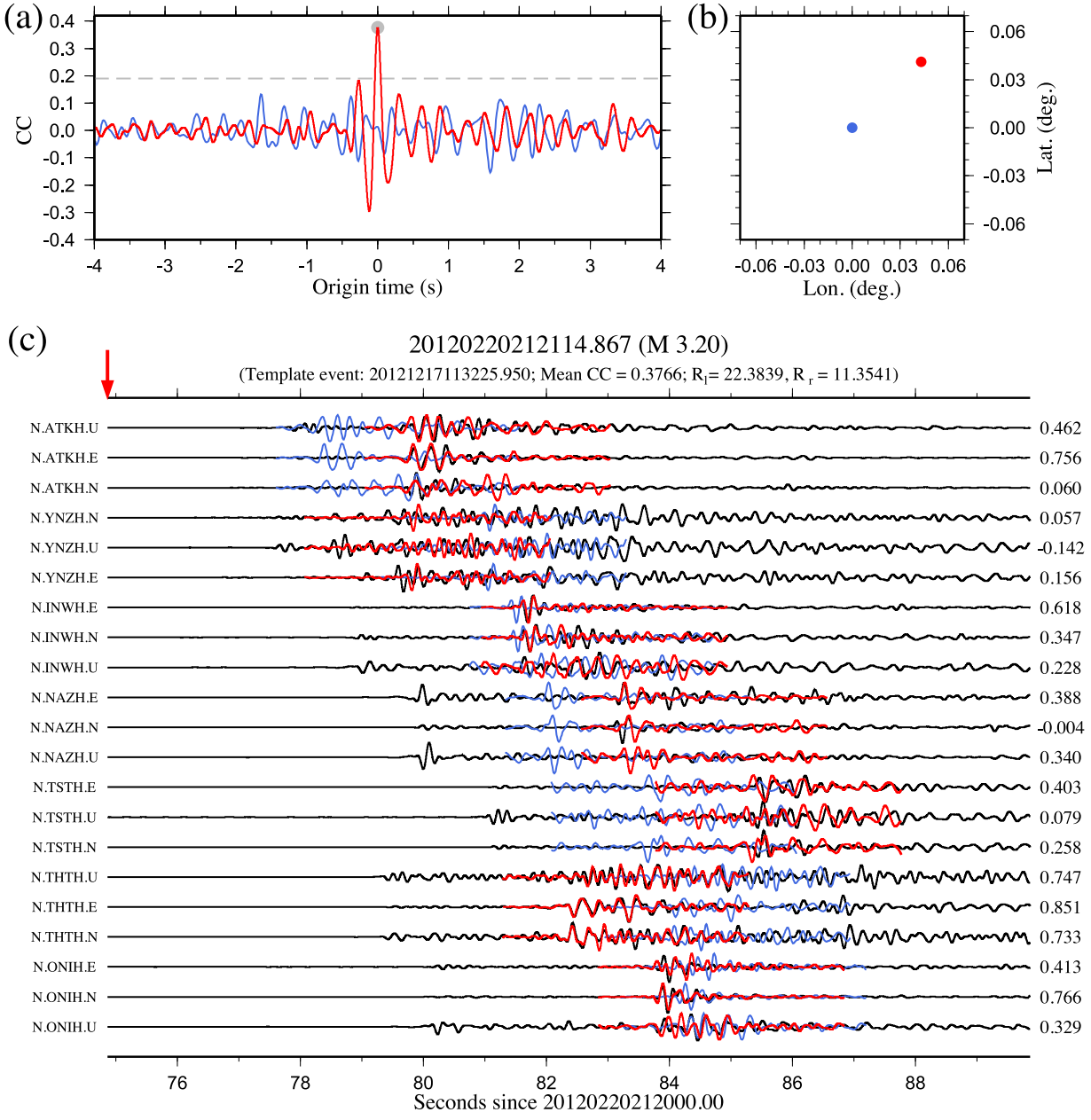

Figure 8. (a) Comparisons of the stacked correlograms, (b) determined slave event location and (c) predicted signal matching to the continuous waveforms (black traces) between the M&L and matched filter methods for a case when the template (black star in Fig. 2a) and slave earthquake (red star in Fig. 2a) are separated by a large distance. Blue symbols or traces are for the matched filter and red for M&L. The grey dashed line in (a) indicates the mean CC threshold (0.19) of detection. Continuous earthquake waveforms in (c) begins with the origin time (red arrow) shown in (a). Station name and CC value are labelled on the left- and right-hand sides of each trace, and the total mean CC and SNRs computed in the M&L method under the subtitle of Fig. 8(c).

location uncertainty would obviously depend on the magnitude of the detected event, the background noise and station coverage. Rather than estimating the uncertainty of individual detection, we quantify the uncertainties of the detections according to the region of occurrence and magnitude of the events, in the context of the recorded background noise. The quantification is to estimate the level of confidence in the spatial distribution of the CC values, by taking reference of relocation results and uncertainty estimates in the traditional method and using seismic data of event pairs and their scale-down signals. For a region, we select an event pair in the region whose traveltimes of the seismic phases can be accurately measured. We estimate their relative location and the uncertainty of the location using the traveltime differences between the event pair based on the method of Wen (2006). These relocation results and uncertainty estimate are well established in the previous studies (Wen 2006; Wen & Long 2010; Zhang & Wen 2013) and are used as references for uncertainty estimate of events of various magnitudes in the same region. For the convenience of discussion, we term them 'the reference location' and 'the reference uncertainty'. To estimate the M&L location uncertainty for various magnitudes of the detected events in the region, we perform the M&L detection procedure with the background noise and the signals of the slave event (one of the event in the event pair) scaled down by factors that are appropriate for various magnitudes. The M&L location uncertainty for a particular magnitude of the detected events in the region is the deviation of the M&L detected location based on the scaled-down signals (that are appropriate for that magnitude) from 'the reference location' plus 'the reference uncertainty'. The minimal CC value (expressed as percentage of the maximum CC value) within the location uncertainty is used to define the location error bar for the detected events of that magnitude.

We elaborate the uncertainty estimates using the examples of slave event 1 above. By applying Wen (2006) method, we determine the best-fitting location of slave earthquake 1 (the reference location) relative to the reference location that minimizes the rms traveltime residual of the Sg phases observed in the stations in Fig. 2(a) between the two earthquakes (Fig. S1), with a horizontal uncertainty (the reference uncertainty) of 50 m (inferred from its 95 per cent confidence ellipses based on the chi-square distribution). We then determine the location of the slave event based on M&L detection. The deviation of the M&L location from the reference location is 15 m. A location uncertainty of 65 m (50 m + 15 m) is thus assigned. The minimal CC value within the location uncertainty of 65 m is 94.5 per cent of the maximal mean CC. The region within 94.5 per cent of the maximal mean CC value is thus defined as the location uncertainty for M&L event detection of events with a magnitude of 3.20, the magnitude of slave event 1. In this example case, such uncertainty region corresponds to an ellipse with a 100-m-long semi-axis centred in the M&L detected location of slave earthquake 1 (Fig. 4).

Following the procedures we mention above, the estimates of location uncertainty for detected events of other magnitudes are performed with the scaled-down slave event signals superimposed with the background noise. The location uncertainties of detected events of $M = 0.2$ (with a scaling factor of 0.001, Fig. 5e), $M = -0.1$ (scaling factor 0.0005, Fig. 5g) and $M = -0.4$ (scaling factor 0.00025, Fig. 5h) are within 88, 87 and 77 per cent of the maximal mean CC value, respectively, corresponding to ellipses with the long semi-axis being 145, 150 and 200 m (Figs S2–S4). Note that, even at the scaled-down $M = -0.4$ earthquake (with a scaling factor of 0.00025), which approaches the M&L detection limit (Fig. 5h), the M&L location still has a resolution of 200 m (Fig. S4).

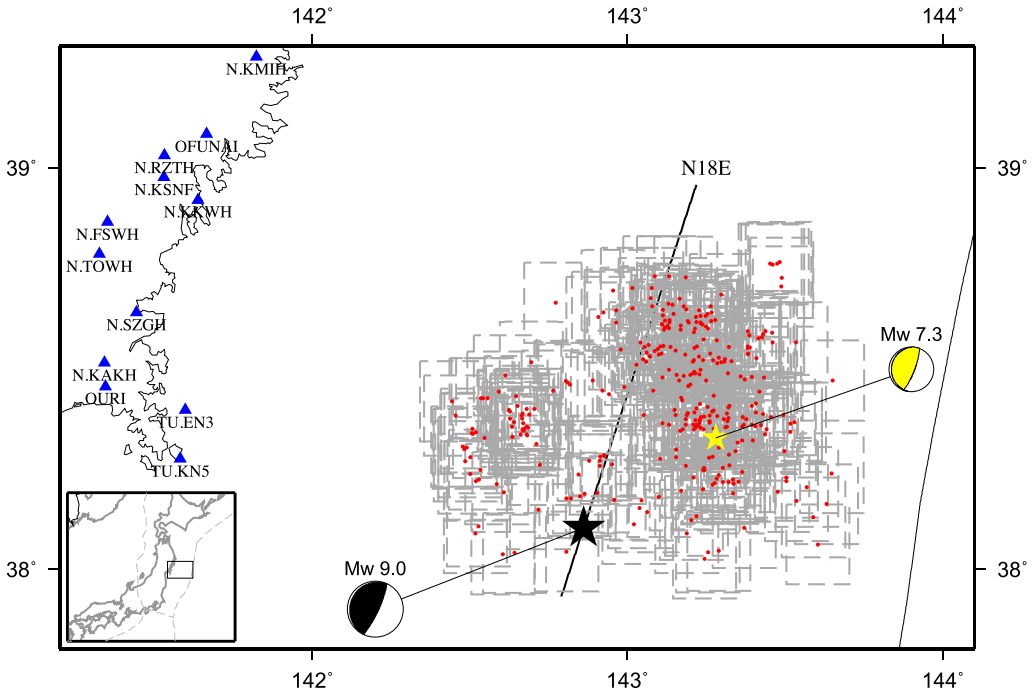

Figure 9. 329 template earthquakes (red dots) and 12 seismic stations (blue triangles) used in the foreshock detection of the M_w 9.0 2011 Tohoku earthquake. The focal mechanisms of the largest M_w 7.3 foreshock (yellow star) and main earthquake (black star) are denoted by yellow/white and black/white spheres, respectively. The searched area is a region of 0.2° × 0.2° (grey rectangles) centred at each template location in the M&L method. The thick black straight line indicates the projection direction in Fig. 13, which is parallel to the Japan Trench (black curve). Inset: the regional map of Japan with the black rectangle indicating the study area.

4 APPLICATION TO FORESHOCK DETECTION BEFORE THE 2011 M_w 9.0 TOHOKU EARTHQUAKE

The foreshock activities may have crucial implications for large earthquake nucleation, earthquake prediction and risk assessment (Thatcher 1989; Ellsworth & Beroza 1995; McGuire *et al.* 2005; Bouchon *et al.* 2011; Brodsky & Lay 2014). The 2011 March 11 M_w 9.0 Tohoku earthquake is well known to be preceded by many foreshocks. According to the JMA catalogue, the seismicity increases since 2011 February 13, and the largest foreshock was a M_w 7.3 event that occurred along the plate interface on 2011 March 9, ~45 km away from the main earthquake (Ide *et al.* 2011). Although the JMA detects many foreshocks based on the dense array, many are missing from its catalogue. Kato *et al.* (2012) applied the matched filter technique using the continuous seismograms of 14 three-component stations along the Pacific coast between 2011 February 13 and March 11 (before the M_w 9.0 main earthquake). More than four times (1416) foreshocks are identified in their study. In this section, we apply the M&L method to detect the missing foreshocks, and compare with the results of the matched filter, under the same data processing procedure and detection threshold.

We collect all 333 earthquakes in the JMA catalogue and the continuous seismograms recorded by 12 open three-component (except for TU.EN3 with two channels) stations along the Pacific coast, from 2011 February 13 to the origin time of the M_w 9.0 main earthquake (Kato *et al.* 2012; Fig. 9). 329 events are chosen as our template events. Four events (20110309161318, 20110309191314, 20110310180219 and 20110311074401) are excluded, because their *S* waves are mingled with the *P* waves of the next larger earthquake at some stations. Data are band-pass filtered from 2 to 8 Hz and Sg waveforms are used. Relocation parameters of Sg phase are calculated using the TauP toolkit (Crotwell *et al.* 1999) based on the 1-D JMA2001 velocity model (Ueno *et al.* 2002). 4-s waveform segments (1 s before and 3 s after the predicted arrival time of Sg wave) are used as the template waveforms. Due to lack of the nearest stations and the strong trade-off between the depth and origin time, the earthquake depth cannot be well constrained (Billings *et al.* 1994; Zhang *et al.* 2014), so we fix the depth to be the templates and just search the potential locations in the horizontal plane, within meshes of 0.2° × 0.2° in longitude and latitude, with a searching interval of 0.01°, centred at each template location (Fig. 9).

To define mean CC and SNR thresholds, we first estimate the background mean CC value from all 329 template self-detections. Both left and right average background CC values of the stacked correlograms are estimated to be 0.03, that is, $\overline{C_l^0} = 0.03$ and $\overline{C_r^0} = 0.03$ (Fig. S5). Detection criteria are chosen empirically as follows based on the eye-checking of relatively large event detections to avoid possible false detection. When the mean CC value is larger than nine times of the background mean CC value (0.27), only the mean

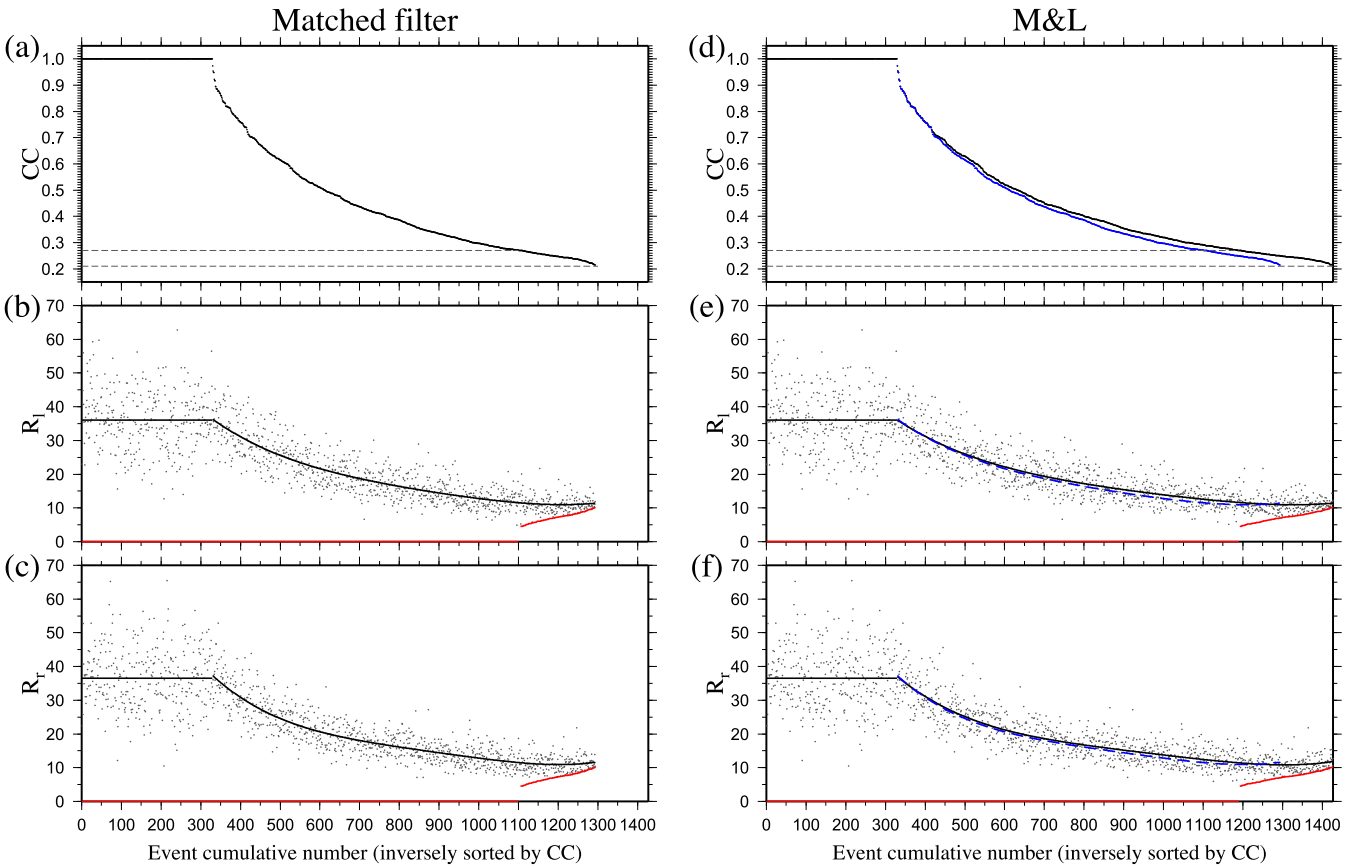

Figure 10. Mean CC and SNRs for the matched filter (a, b, c) and M&L (d, e, f) as a function of number of the detected events inversely sorted by mean CC values. Black straight lines correspond to 329 template self-detections. The black fitting curves in (b) and (e) are for the left SNRs (R_l), and (c) and (f) for the right SNRs (R_r). Blue dotted line in (b) corresponds to the black dotted line in (a), and blue dashed lines in (e)–(f) correspond to the black fitting lines in (b)–(c). The dashed lines in (a) and (d) indicate the segmented mean CC thresholds 0.27 and 0.21, where the left and right SNR coefficients α_l and α_r change in SNR threshold (Fig. S5). Red lines in (b)–(c) and (e)–(f) denote the SNR thresholds of event detections.

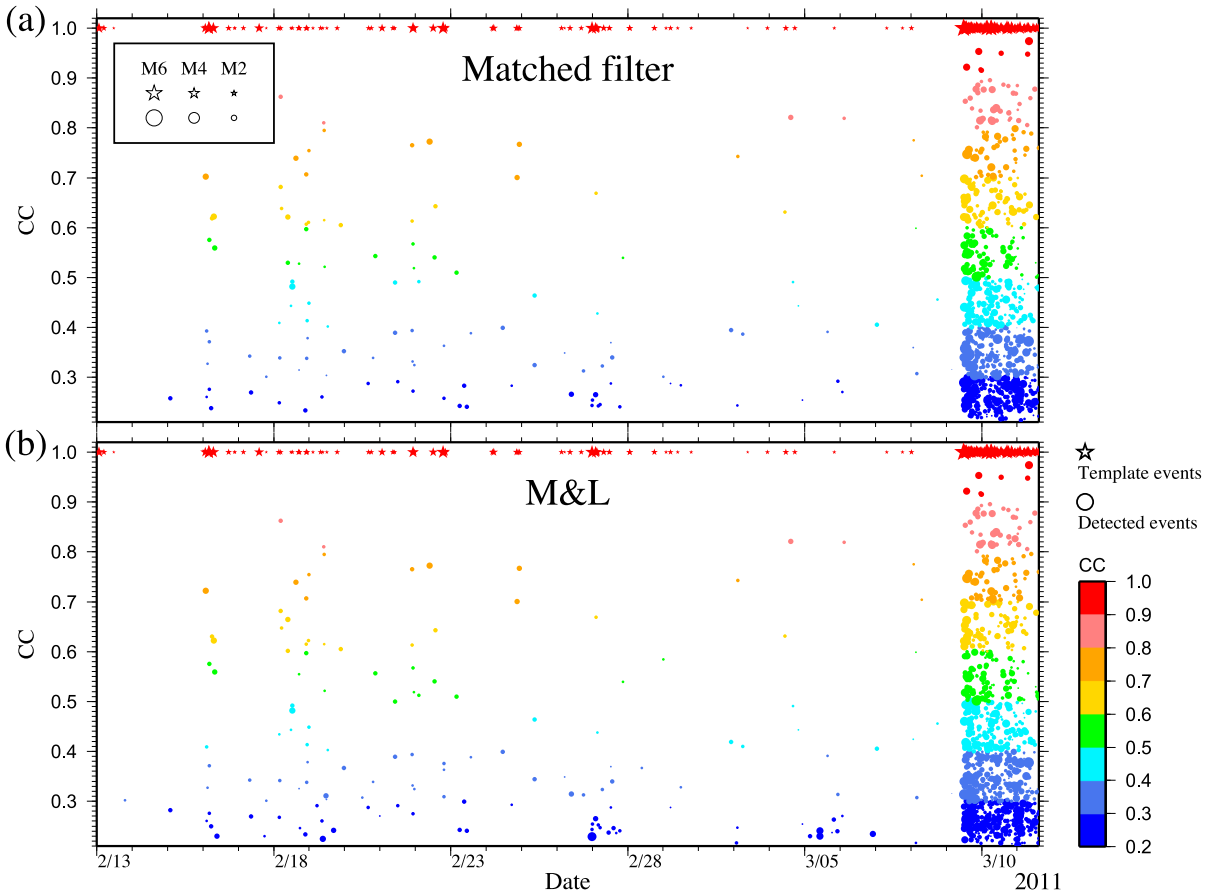

Figure 11. Mean CC values of the detected events from 2011 February 13 to the 2011 March 11 main shock for the matched filter (a) and M&L (b). The detected events (circles) and templates (stars) are scaled to the magnitudes and colour-coded by the mean CC values.

CC threshold is used. Both the mean CC and SNR thresholds are applied when mean CC value is larger than seven times (0.21) and smaller than nine times (0.27) of the background mean CC. In the SNR threshold setting, α_l and α_r are set to decrease linearly from 1.5 to 0.5 when mean CC increases from seven times of the background mean CC to nine times of the background mean CC (Figs 10 and S5).

We detect 1427 foreshock events, four times more than the number of the template events. Under the same thresholds, we detect 1293 events using the matched filter method (Figs 10 and 11). All 329 templates are recovered by both methods with mean CC values of 1.0 (Figs 10 and 11). For the other events detected by the both methods, both the mean CC values and SNRs are higher in the M&L detection than the matched filter (Figs 10 and 11). The M&L method detects 9 per cent (134) more events than the matched filter method (Fig. 12a). 41 per cent (580) of the total detected events are not co-located with the template locations (Fig. 12b). The histogram of event separation from the template events are shown in Fig. 12(c), with the largest event separation (event 20110311003119 with template 20110310001424) being 9.4 km. In contrast, the matched filter method fails to identify events that are ∼4 km away from the template events.

We project all the identified events along N18E, the orientation of the Japan Trench axis (Shao *et al.* 2011; Fig. 9). The space–time migration of the foreshocks illustrates the seismicity sequence expansion with five segments in the trench-parallel direction for both the matched filter and M&L results (Fig. 13), which is quite different from the result of Kato *et al.* (2012), because of the difference of projection angle and detected seismicity. The introduction of SNR threshold in our study improves the detection ability distinctly, especially for the time window between 2011 March 3 and March 8, which provides more detailed event information to estimate foreshock migration in our study than Kato *et al.* (2012). The migration sequence started on 16 February at a speed of ∼2.3 km d^{-1} and ended on 23 February, and stayed 20 km away from the epicentre of main shock in the later 5 d (from 23 February to 27 February), then jumped to ∼1 km close to the epicentre and kept activity between 27 February and 2 March (Fig. 13). After 1 d pause, earthquake sequence moved back at a speed of 5.5 km d^{-1} towards to the direction of the M_w 7.3 foreshock (Fig. 13). After the M_w 7.3 event, the migration sequence broke out at an average speed of ∼25 km d^{-1}, and the migration front slowed down diffusively with time (Fig. 13), which supports the speculation that the M_w 9.0 main earthquake was triggered by diffusional propagation of after-slip from the M_w 7.3 foreshock (Ando & Imanishi 2011). The complex foreshock migration could provide significant observational constraints on the mechanism and dynamic process of large earthquake triggering.

5 DISCUSSION

The M&L method differs from commonly used detection algorithms, the SSA and matched filter. The M&L method differs from SSA method in two aspects: (1) the M&L method stacks the correlograms between template waveform and potential small-event waveform by scanning through the space and time, while the SSA method stacks the seismic amplitude or envelope. The waveform

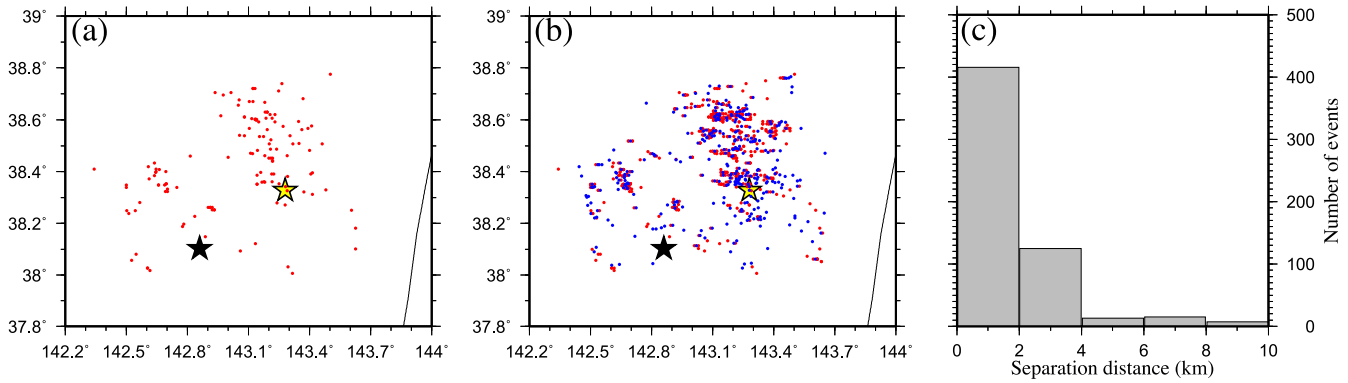

Figure 12. (a) 134 events (9 per cent of the total) detected by M&L (red circles), but not by the matched filter. (b) 580 (41 per cent of the total) detected events (red circles) that are not located at the template locations (blue circles). (c) Histogram of separation distance of slave event from the template for the detected events in (b). The largest M_w 7.3 foreshock and the M_w 9.0 main shock are marked by yellow and black stars in (a) and (b), while the black curve indicates the boundary of Japan Trench.

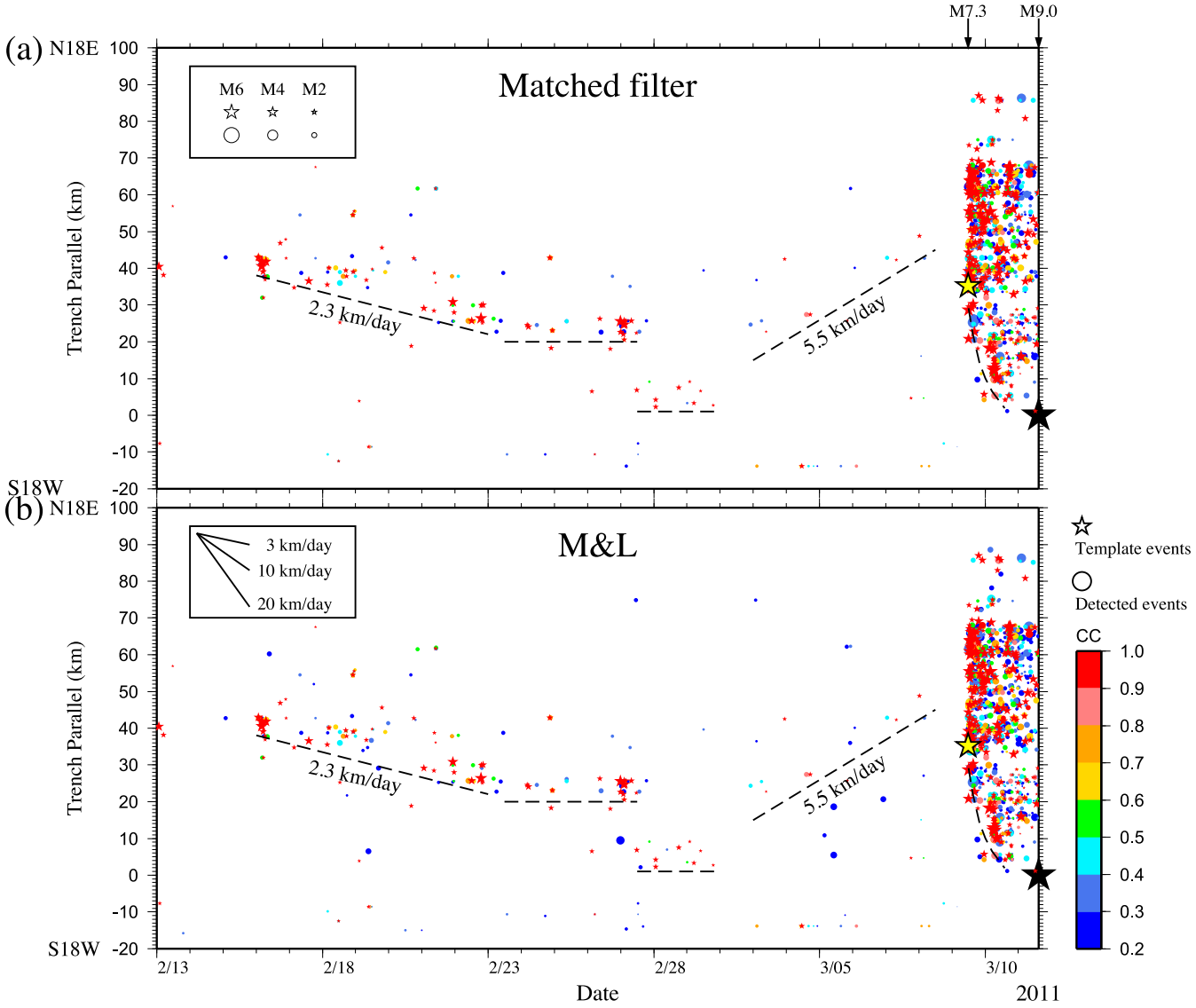

Figure 13. Spatial-temporal migration of the foreshocks between 2011 February 13 and the origin time of the main shock detected by the matched filter (a) and M&L (b). All earthquake locations are projected along the trench axis shown in Fig. 9. The detected events (circles) and templates (stars) are scaled to the magnitudes, and colour-coded by the mean CC values. Five migration sequences (marked by black dashed lines) are observed based on the temporal and spatial changes of the detected earthquakes.

correlation is much more sensitive in detecting the weak signal than the methods of identifying energy from seismic amplitude or envelope (Fig. 5). (2) Unlike the SSA method, which uses the absolute time in relocation, the M&L method utilizes the traveltime difference due to the location difference between the template and potential small-magnitude event. The absolute traveltime is affected by the accuracy of the velocity model used, but the traveltime difference between the events is only sensitive to the average velocity structure between the events. Thus, unlike the SSA method, the detection ability of the M&L method depends only weakly on the accuracy of the velocity model.

The M&L method differs from the matched filter method in one key aspect: the M&L method does not assume that the small-magnitude events are colocated with the template events and the method searches for an optimal location of the small-magnitude event over possible candidate locations. In this regard, the M&L method places event detection to a lower magnitude level than the matched filter method and, at the same time, provides high-precision location information of the detected small-magnitude events. Although there are some attempts to consider possible arrival time difference between the template event and small-magnitude events in the matched filter method, for example, Shelly *et al.* (2007) shift the correlograms to align their maximal values within a limited time window (0.4 s) before stacking and define such detection as the 'weak' detection, these alignments are done empirically. These empirical alignments of correlograms do not take into account of consistency of physics of wave propagation and the seismic energy does not necessarily correspond to the maximum correlation values when the SNR is high. These empirical alignments may on the other hand also increase the chance of false detection.

While, in principle, there is no limit on the distance separation of the small-magnitude event that can be detected from the template, in reality, waveform similarities decrease as the event separation increases, depending on the local heterogeneous structure (Nakahara 2004). For the region we study, the largest distance separation of detectable small events from the template is about ∼10 km.

6 CONCLUSIONS

We present a M&L method for low-magnitude event detection. The M&L method employs some template events and detects small events through stacking cross-correlograms between waveforms of the template events and potential small event signals in the continuous waveforms over multiple stations and components. The stacked correlograms are examined over potential small event locations scanning through a 3-D region around the template, by making relative traveltime corrections based on the relative locations of the template event and the potential small event before stacking. The M&L method differs from commonly used detection algorithms, SSA and matched filter. The M&L method differs from the SSA method in two aspects: (1) the M&L method employs waveform correlograms, instead of seismic amplitude or envelope in event detection and (2) the M&L method utilizes the traveltime difference due to the location difference between the template and potential small-magnitude event, rather than the absolute traveltime. These two aspects make the M&L method much more sensitive in detecting the weak signal and less dependent on the accuracy of the velocity models used. Unlike the matched filter method, which assumes small events are colocated with the template events, the M&L method searches for an optimal location of the small-magnitude event over possible candidate locations, placing event detection to a lower magnitude level and simultaneously providing high-precision location information of the detected small-magnitude events.

We illustrate the effectiveness of the M&L method and its comparison with the matched filter method using the observed waveforms of three earthquakes occurring in the Japan Island as well as the recorded background noise. The M&L method places event detection to a much smaller magnitude than the matched filter and is able to detect events that have large distance separations from the template (>4 km) when the matched filter fail. As an example of application and further comparison, we apply the M&L and matched filter methods to detect the foreshocks before the 2011 M_w 9.0 Tohoku earthquake. The M&L method detects four times more events (1427) than the templates and 9 per cent (134) more than the matched filter under the same detection threshold. Up to 41 per cent (580) of the events detected by the M&L method are not co-located at the template locations with the largest event separation of 9.4 km. Based on the foreshock activity we identify, five migration sequences are observed along the trench-parallel direction toward the epicentre of the M_w 9.0 main shock in space–time.

ACKNOWLEDGEMENTS

We thank the National Research Institute for Earth Science and Disaster Prevention (NIED), Tohoku University and JMA for providing their seismic data. We think Aitaro Kato for sharing the template catalogue and stations used in their study and Zhigang Peng for useful discussions. This paper benefited significantly from the reviews by editor Joachim Wassermann and two anonymous reviewers. This work was supported by the National Natural Science Foundation of China under Grants NSFC41130311 and the Chinese Academy of Sciences and State Administration of Foreign Experts Affairs International Partnership Program for Creative Research Teams.

REFERENCES

Ando, R. & Imanishi, K., 2011. Possibility of M (w) 9. 0 mainshock triggered by diffusional propagation of after-slip from M (w) 7. 3 foreshock, *Earth, Planets Space,* **63,** 767–771.

Anikiev, D., Valenta, J., Staněk, F. & Eisner, L., 2014. Joint location and source mechanism inversion of microseismic events: benchmarking on seismicity induced by hydraulic fracturing, *Geophys. J. Int.*, **198**(1), 249–258.

Billings, S., Kennett, B.L. & Sambridge, M.S., 1994. Hypocentre location: genetic algorithms incorporating problem specific information, *Geophys. J. Int.,* **118,** 693–706.

Bouchon, M., Karabulut, H., Aktar, M., Özalaybey, S., Schmittbuhl, J. & Bouin, M.-P., 2011. Extended nucleation of the 1999 Mw 7.6 Izmit earthquake, *Science,* **331,** 877–880.

Brodsky, E.E. & Lay, T., 2014. Recognizing Foreshocks from the 1 April 2014 Chile Earthquake, *Science,* **344,** 700–702.

Cao, W., Schuster, G.T., Zhan, G., Hanafy, S.M. & Boonyasiriwat, C., 2008. Demonstration of super-resolution and super-stacking properties of time reversal mirrors in locating seismic sources, in *Proceedings of the 78th Annual International Meeting,* pp. 3018–3022.

Crotwell, H.P., Owens, T.J. & Ritsema, J., 1999. The TauP Toolkit: flexible seismic travel-time and ray-path utilities, *Seismol. Res. Lett.,* **70,** 154–160.

Dreger, D. & Kaverina, A., 2000. Seismic remote sensing for the earthquake source process and near source strong shaking: a case study of the October 16, 1999 Hector Mine earthquake, *Geophys. Res. Lett.,* **27,** 1941–1944.

Drew, J., White, R.S., Tilmann, F. & Tarasewicz, J., 2013. Coalescence microseismic mapping, *J. geophys. Int.,* **195,** 1773–1785.

Eisner, L., Abbott, D., Barker, W.B., Lakings, J. & Thornton, M.P., 2008. Noise suppression for detection and location of microseismic events using a matched filter, in *Proceeding of the 2008 SEG Annual Meeting*.

Ellsworth, W. & Beroza, G., 1995. Seismic evidence for an earthquake nucleation phase, *Science,* **268,** 851–855.
Gharti, H.N., Oye, V., Roth, M. & Kühn, D., 2010. Automated microearthquake location using envelope stacking and robust global optimization, *Geophysics,* **75,** MA27–MA46.
Gibbons, S.J. & Ringdal, F., 2006. The detection of low magnitude seismic events using array-based waveform correlation, *Geophys. J. Int.,* **165,** 149–166.
Gibbons, S.J., Bøttger Sørensen, M., Harris, D.B. & Ringdal, F., 2007. The detection and location of low magnitude earthquakes in northern Norway using multi-channel waveform correlation at regional distances, *Phys. Earth planet. Inter.,* **160,** 285–309.
Gomberg, J., Reasenberg, P., Bodin, P. & Harris, R., 2001. Earthquake triggering by seismic waves following the Landers and Hector Mine earthquakes, *Nature,* **411,** 462–466.
Grigoli, F., Cesca, S., Amoroso, O., Emolo, A., Zollo, A. & Dahm, T., 2013a. Automated seismic event location by waveform coherence analysis, *Geophys. J. Int.,* **196,** 1742–1753.
Grigoli, F., Cesca, S., Vassallo, M. & Dahm, T., 2013b. Automated seismic event location by travel-time stacking: an application to mining induced seismicity, *Seismol. Res. Lett.,* **84,** 666–677.
Hanafy, S.M., Cao, W., McCarter, K. & Schuster, G.T., 2009. Using superstacking and super-resolution properties of time-reversal mirrors to locate trapped miners, *Leading Edge,* **28,** 302–307.
Helmberger, D.V., 1983. Theory and application of synthetic seismograms, in *Earthquakes: Observation, Theory and Interpretation,* pp. 174–222, eds Kanamori, H. & Boschi, E., Soc. Italiana di Fisica.
Hill, D. *et al.* 1993. Seismicity remotely triggered by the magnitude 7.3 Landers, California, earthquake, *Science,* **260,** 1617–1623.
House, L., 1987. Locating microearthquakes induced by hydraulic fracturing in crystalline rock, *Geophys. Res. Lett.,* **14,** 919–921.
Ide, S., Baltay, A. & Beroza, G.C., 2011. Shallow dynamic overshoot and energetic deep rupture in the 2011 Mw 9.0 Tohoku-Oki earthquake, *Science,* **332,** 1426–1429.
Kao, H. & Shan, S.-J., 2004. The Source-Scanning Algorithm: mapping the distribution of seismic sources in time and space, *Geophys. J. Int.,* **157,** 589–594.
Kao, H. & Shan, S.-J., 2007. Rapid identification of earthquake rupture plane using Source-Scanning Algorithm, *Geophys. J. Int.,* **168,** 1011–1020.
Kato, A., Obara, K., Igarashi, T., Tsuruoka, H., Nakagawa, S. & Hirata, N., 2012. Propagation of slow slip leading up to the 2011 Mw 9.0 Tohoku-Oki earthquake, *Science,* **335,** 705–708.
Kilb, D., Gomberg, J. & Bodin, P., 2000. Triggering of earthquake aftershocks by dynamic stresses, *Nature,* **408,** 570–574.
Kuge, K., 2003. Source modeling using strong-motion waveforms: toward automated determination of earthquake fault planes and moment-release distributions, *Bull. seism. Soc. Am.,* **93,** 639–654.
Langet, N., Maggi, A., Michelini, A. & Brenguier, F., 2014. Continuous Kurtosis-based migration for seismic event detection and location, with application to piton de la Fournaise Volcano, La Reunion, *Bull. seism. Soc. Am.,* **104,** 229–246.
Liao, Y.-C., Kao, H., Rosenberger, A., Hsu, S.-K. & Huang, B.-S., 2012. Delineating complex spatiotemporal distribution of earthquake aftershocks: an improved source-scanning Algorithm, *Geophys. J. Int.,* **189,** 1753–1770.
McGuire, J.J., Boettcher, M.S. & Jordan, T.H., 2005. Foreshock sequences and short-term earthquake predictability on East Pacific Rise transform faults, *Nature,* **434,** 457–461.
Meng, X., Peng, Z. & Hardebeck, J.L., 2013. Seismicity around Parkfield correlates with static shear stress changes following the 2003 Mw 6.5 San Simeon earthquake, *J. geophys. Res.: Solid Earth,* **118,** 3576–3591.
Meng, X. & Peng, Z., 2014. Seismicity rate changes in the Salton Sea Geothermal Field and the San Jacinto Fault Zone after the 2010 Mw 7.2 El Mayor-Cucapah earthquake, *Geophys. J. Int.,* **197,** 1750–1762.
Mori, J. & Hartzell, S., 1990. Source inversion of the 1988 Upland, California, earthquake: determination of a fault plane for a small event, *Bull. seism. Soc. Am.,* **80,** 507–518.
Nakahara, H., 2004. Correlation distance of waveforms for closely located events-I. Implication of the heterogeneous structure around the source region of the 1995 Hyogo-Ken Nanbu, Japan, earthquake (Mw = 6.9), *Geophys. J. Int.,* **157,** 1255–1268.
Peng, Z. & Zhao, P., 2009. Migration of early aftershocks following the 2004 Parkfield earthquake, *Nat. Geosci.,* **2,** 877–881.
Peng, Z., Hill, D.P., Shelly, D.R. & Aiken, C., 2010. Remotely triggered microearthquakes and tremor in central California following the 2010 Mw 8.8 Chile earthquake, *Geophys. Res. Lett.,* **37**, L24312, doi:10.1029/2010GL045462.
Richards, P.G. & Kim, W.-Y., 1997. Testing the nuclear test-ban treaty, *Nature,* **389,** 781–782.
Rutledge, J.T. & Phillips, W.S., 2003. Hydraulic stimulation of natural fractures as revealed by induced microearthquakes, Carthage Cotton Valley gas field, east Texas, *Geophysics,* **68,** 441–452.
Shao, G., Li, X., Ji, C. & Maeda, T., 2011. Focal mechanism and slip history of the 2011 Mw 9.1 off the Pacific coast of Tohoku Earthquake, constrained with teleseismic body and surface waves, *Earth, Planets Space,* **63,** 559–564.
Shearer, P.M. & Astiz, L., 1997. Locating nuclear explosions using waveform cross-correlation, in *Proceedings of the 19th Ann. Seis. Res. Symp. Mon. CTBT,* pp. 301–309.
Shelly, D.R., 2010. Migrating tremors illuminate complex deformation beneath the seismogenic San Andreas fault, *Nature,* **463,** 648–652.
Shelly, D.R., Beroza, G.C., Ide, S. & Nakamula, S., 2006. Low-frequency earthquakes in Shikoku, Japan, and their relationship to episodic tremor and slip, *Nature,* **442,** 188–191.
Shelly, D.R., Beroza, G.C. & Ide, S., 2007. Non-volcanic tremor and low-frequency earthquake swarms, *Nature,* **446,** 305–307.
Thatcher, W., 1989. Earthquake recurrence and risk assessment in circum-Pacific seismic gaps, *Nature,* **341,** 432–434.
Ueno, H., Hatakeyama, S., Aketagawa, T., Funasaki, J. & Hamada, N., 2002. Improvement of hypocenter determination procedures in the Japan Meteorological Agency, *Q. J. Seismol,* **65,** 123–134.
Waldhauser, F., Schaff, D., Richards, P.G. & Kim, W.-Y., 2004. Lop Nor revisited: underground nuclear explosion locations, 1976–1996, from double-difference analysis of regional and teleseismic data, *Bull. seism. Soc. Am.,* **94,** 1879–1889.
Wen, L., 2006. localized temporal change of the Earth's inner core boundary, *Science,* **314,** 967–970.
Wen, L. & Long, H., 2010. High-precision location of North Korea's 2009 nuclear test, *Seismol. Res. Lett.,* **81,** 26–29.
Yang, H., Zhu, L. & Chu, R., 2009. Fault-plane determination of the 18 April 2008 Mount Carmel, Illinois, earthquake by detecting and relocating aftershocks, *Bull. seism. Soc. Am.,* **99,** 3413–3420.
Zhang, M. & Wen, L., 2013. High precision location and yield of North Korea's 2013 nuclear test, *Geophys. Res. Lett.,* **40,** 2941–2946.
Zhang, M., Tian, D. & Wen, L., 2014. A new method for earthquake depth determination: stacking multiple-station autocorrelograms, *Geophys. J. Int.,* **197,** 1107–1116.

SUPPORTING INFORMATION

Additional Supporting Information may be found in the online version of this article:

Figure S1. Rms traveltime residuals as a function of relative location of slave event 1 (colour maps, only the regions with the values less than 35 ms are plotted), the best-fitting location of the slave event (blue stars, the points of the minimal rms traveltime residual of the Sg phases observed in the stations in Fig. 2(a) between the two earthquakes) relative to the template location (black stars) in three plane views: (a) longitude–latitude plane, (b) latitude–depth plane and (c) longitude–depth plane, along with the 95 per cent confidence level for the slave earthquake location based on the chi-square distribution (black ellipses). Grey stars are the locations of slave earthquake 1 determined by JMA.

Figure S2. Same as Fig. 4, except that slave earthquake 1 is scaled-down to be an equivalent magnitude $M = 0.2$ event (with a scaling factor of 0.001). White ellipses represent the determined confidence level of the scaled-down slave earthquake 1 location, within 88 per cent of the maximal mean CC.

Figure S3. Same as Fig. 4, except that slave earthquake 1 is scaled-down to be an equivalent magnitude $M = -0.1$ event (with a scaling factor of 0.0005). White ellipses represent the determined confidence level of the scaled-down slave earthquake 1 location, within 87 per cent of the maximal mean CC.

Figure S4. Same as Fig. 4, except that slave earthquake 1 is scaled-down to be an equivalent magnitude $M = -0.4$ event (with a scaling factor of 0.00025). White ellipses represent the determined confidence level of the scaled-down slave earthquake 1 location, within 77 per cent of the maximal mean CC.

Figure S5. (a) Stacked cross-correlograms (grey traces) for all 329 template self-detections and definitions of the background mean CC values and SNRs. $\overline{C_l^0}$ and $\overline{C_r^0}$ are defined as the background mean CC values in the time windows on the left and right of the maximum value of the correlograms. $R_l(t)$ and $R_r(t)$ are the left and right SNRs of the stacked correlogram at a given time t (here t equals to zero) relative to the average CC values obtained at times in the left and right vicinities. (b) The left and right SNR coefficients α_l and α_r as a function of mean CC value. Only mean CC threshold is applied when mean CC is larger than nine times of the background mean CC, that is, α_l and α_r are zero when mean CC is larger than 0.27. In the SNR threshold setting for the case of lower CC values, coefficients α_l and α_r increase linearly from 0.5 to 1.5 when mean CC decreases from 0.27 (corresponding to nine times of the background mean CC) to 0.21 (corresponding to seven times of the background mean CC) (http://gji.oxfordjournals.org/lookup/suppl/doi:10.1093/gji/ggu466/-/DC1).